Nanochem. Res., 8(4): 278-286, Autumn 2023

RESEARCH PAPER

Visible Light Photodegradation of Methyl Orange Using α-Fe_2O_3 Nanoparticles Synthesized via Solvothermal Method in Presence of PVP

Aliakbar Dehno Khalaji*, Elham Sadat Zeinoddin, Ali Ghorbani Khorshidi, Ahmad Ghaffari

Department of Chemistry, Faculty of Science, Golestan University, Gorgan, Iran

ARTICLE INFO

Article History:
Received 31 May 2023
Accepted 03 Sep 2023
Published 01 Oct 2023

Keywords:
Spherical Fe_2O_3 nanoparticles,
Solvothermal,
Photocatalytic MO degradation

ABSTRACT

In this study, hematite (α-Fe_2O_3) nanoparticles were synthesized *via* solvothermal route and their photocatalytic activity for the degradation of methyl orange (MO) under visible light was studied. The iron precursors solution were prepared by dissolving $Fe(NO_3)_3{\cdot}9H_2O$ or $Fe_2(SO_4)_3$ in an acetic acid glacial/ethanol (9:1 v/v) mixture followed by the addition of polyvinylpyrrolidone (PVP) and urea. The as-prepared α-Fe_2O_3 nanoparticles were characterized by X-ray diffraction (XRD), vibrating sample magnetometer (VSM), Brunauer-Emmett-Teller (BET), and transmission electron microscope (TEM) techniques. The characterization results confirmed that the α-Fe_2O_3 nanoparticles were successfully prepared which had ferromagnetic behavior and micropores with quasi-spherical shapes. The effect of initial pH solution, contact time, and photocatalyst dosage on the photocatalytic degradation of MO was investigated. The photocatalytic results showed the degradation efficiency of 84.3% and 96.8% for MO, after 120 min of visible light irradiation. The photocatalytic examinations illustrated that the degradation of MO follows Langmuir kinetic model with the rate constant (k) of 0.01374 and 0.02689 min^{-1}, respectively.

How to cite this article
Dehno Khalaji A., Zeinoddin E. S., Ghorbani Khorshidi A., Ghaffari A., Visible light photodegradation of methyl orange using α-Fe_2O_3 nanoparticles synthesized via solvothermal method in presence of PVP. Nanochem. Res., 2023; 8(4): 278-286.
DOI: 10.22036/NCR.2023.04.06

INTRODUCTION

In recent years, the use of different metal oxide nanoparticles as photocatalysts is a common route for the degradation of various organic dyes such as direct black 112 [1], congo red [2], reactive blue 21 [3], and methyl orange [4]. Among different metal oxides, iron oxide hold significant importance. It has three main phases: FeO, Fe_2O_3 and Fe_3O_4. These phases are known as crucial materials due to their unique properties and application [5-9]. Hematite (α-Fe_2O_3) stands out as an excellent iron oxide nanoparticles due to its stability, affordability, biocompatibility, eco-friendly properties, and remarkable photocatalytic ability to degrade various organic dyes [10-21]. Today, in all countries, due to the increase in pollution and also incredibly polluted different water sources, the availability of drinking water is limited and has become one of the major problems [10]. Various heavy meal oxides and organic dyes are released to the environment due to industrial activities, among which dyes are the most common source of pollution in wastewater [10-32]. Generally, the organic dyes have aromatic azo complex structure characterized by their high stability, water solubility, tendency to inhibit sunlight penetration, non-biodegradability, high toxicity, and also being potentially mutagenic and carcinogenic [10-21]. Methyl orange (MO) as anionic dye (Scheme 1) is used in textile and

* Corresponding Author Email: *alidkhalaji@yahoo.com*

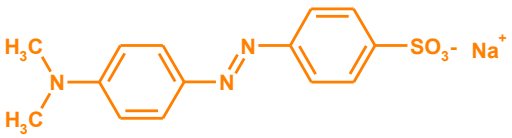

Scheme 1. Chemical structure of methyl orange (MO) dye

printing [13]. Usually, the factories wastewaters contain 10-20% of residual organic dyes usage [17]. Results showed that a small amount of dyes in water can affect its transparency, oxygen solubility, and hence preventing photosynthesis [13]. Thus, the removal of dyes from industrial wastewaters has drawn great attention from many researchers [22-32]. Recently, photodegradation of organic dyes by using metal oxide semiconductors such as CuO [33], Gd_2O_3 [34], $SrFe_{12}O_{19}$ [35-37], CeO_2 [38,39], $NiFe_2O_4$ [40], $CoFe_2O_4$ [41], and Fe_2O_3 [10-21] is widely explored as a highly economical and ecofriendly technique. For example, in their study, Araujo et al. [16] reported the photodegradation of methylene blue (MB) and crystal violet (CV) using α-Fe_2O_3 nanofibers under visible light, which showed the maximum degradations of 66% and 92% for MB and CV, respectively. Mesoporous iron oxide nanowires, as prepared by Gandha et al. [20], demonstrated an efficient methyl orange (MO) and rhodamine B (RhB) photodegradation within 90 min irradiation. In another study, Gupta et al. [14] synthesized coral-like α-Fe_2O_3 nanoparticles for methylene blue (MB), bromo green (BG), methyl orange (MO) and methyl red (MR) photodegradation. Taghavi Fardood et al. [42] synthesized α-Fe_2O_3 (hematite) nanoparticles using Arabic gum (AG) as a biotemplate source by the sol-gel method and used them as a new photocatalyst for the degradation of the Congo red dye. Khalaji et al. [18] prepared α-Fe_2O_3 nanoparticles by wet chemical precipitation technique for the photodegradation of methyl orange (MO) under visible light irradiation. Keerthana et al. [17] applied pure α-Fe_2O_3 nanoparticles in the photodegradation of methylene blue (MB). Therefore, these reports have confirmed that the great interest in the preparation of different shapes of α-Fe_2O_3 nanoparticles used as photocatalysts for various dyes degradation because of their efficiency and reusability [10-21]. However, the agglomeration of α-Fe_2O_3 nanoparticles during the synthesis process is a disadvantage that may increase their final cost [16].

In this work, we synthesized α-Fe_2O_3 nanoparticles using hydrothermal method for application in the photocatalytic degradation of and MO dye under visible light irradiation.

EXPERIMENTAL

Material and methods

$Fe(NO_3)_3{\cdot}9H_2O$, $Fe_2(SO_4)_3$, polyvinyl pyrrolidone (PVP), urea, glacial acetic acid, ethanol, and methyl orange (MO) were purchased from Merck and Aldrich and used without further purification in the synthesis of hematite (α-Fe_2O_3) nanoparticles. The crystalline structure of hematite (α-Fe_2O_3) nanoparticles was studied by X-ray Diffraction (XRD-6000, Shimadzu) using CuKα radiation source (λ=1.5404 Å), from 10-70°. The morphology of hematite (α-Fe_2O_3) nanoparticles was investigated using a JEOL 2011 transmission electron microscope (TEM) with an accelerating voltage of 200 kV. Magnetic property was performed using a vibrating-sample magnetometer (VSM). The UV-Vis spectrum was done using a Perkin-Elmer spectrophotometer. A 300 W xenon lamp with a 420 nm cutoff filter was employed as a visible light source. Brunauer-Emmett-Teller (BET) analysis (N_2 adsorption-desorption isotherms) were measured at 77 K in Gemini series Micrometritics 2360 instrument.

Preparation of hematite (α-Fe_2O_3) nanoparticles

In this work, hematite (α-Fe_2O_3) nanoparticles were synthesized using the hydrothermal technique. Initially, 2 g of $Fe(NO_3)_3{\cdot}9H_2O$ or $Fe_2(SO_4)_3$ was dissolved in 50 mL of ethanol/ glacial acetic acid (45:5 v/v) under magnetic stirring for 10 min. Then, 2 g of PVP was dissolved in 20 mL of distilled water and the mixture was stirred for 1.5 h at 80 °C followed by adding 2 g urea. Finally, the solution was transferred into a Teflon-lined stainless steel autoclave and heated at 150 °C for 24 h. The resulting dark-red precipitates was separated using centrifugation, washed, dried, and finally calcined at 600 °C for 3 h.

Photocatalytic activity studies

The photocatalytic activity of the as-prepared hematite (α-Fe_2O_3) nanoparticles was studied at room temperature using the photodegradation of methyl orange (MO) dye under visible light irradiation at a pH range of 2-7. For each test, a suitable amount of α-Fe_2O_3 nanoparticles (0.005, 0.01 and 0.02 g) as photocatalyst was dispersed in 50 mL of MO solution (20 ppm). The solution

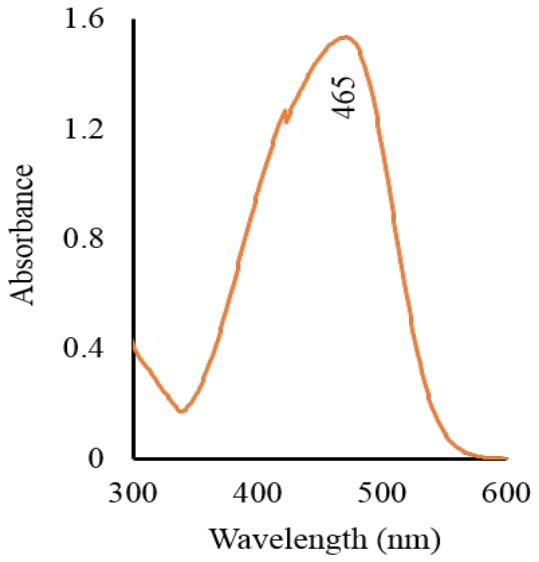

Fig. 1. UV-Vis spectrum of MO dye solution

was kept about 0.5 h under stirring in the dark to ensure the adsorption/desorption equilibrium between MO molecules and the surface of α-Fe_2O_3 nanoparticles. After that, the solution was exposed to visible light for about 90 min. At given times, 5 mL of the mixture was collected, centrifuged, and then its absorption was detected by UV-Vis spectroscopy at 465 nm. The UV-Vis spectrum of MO dye solution is shown in Fig. 1.

RESULTS AND DISCUSSION

Characterization of α-Fe_2O_3 nanoparticles

The XRD patterns of the as-prepared α-Fe_2O_3 nanoparticles are shown in Fig. 2. It can be seen that many peaks are observed at 2θ values of about 24.2°, 33.1°, 35.7°, 49.5°, 54.1°, 57.6°, 62.5° and 64.1° corresponding to the crystal planes of (012), (104), (110), (113), (024), (116), (018), (214), and (300), respectively, which match well with the rhombohedral structure of hematite α-Fe_2O_3 nanoparticles (JCPDS No. 33-0664) [5,9,10,15]. Additionally, the XRD patterns show well crystalline samples (high intensity peaks) without any impurity peaks, confirming the high purity of the synthesized α-Fe_2O_3 nanoparticles. The average crystalline sizes of 35 and 23 nm were calculated for the as-synthesized α-Fe_2O_3 nanoparticles prepared from $Fe(NO_3)_3{\cdot}9H_2O$, and $Fe_2(SO_4)_3$, respectively, by Scherrer equation, $D = 0.94\lambda/\beta\cos\theta$ [19,42,43] from the peak observed at 35.7° (104), where D is the average crystalline size (nm), β is the (FWHM), λ is the X-ray wavelength source Cu$K\alpha$ (1.54 Å), and the θ is the Bragge angle.

Fig. 3 show the *M-H* hysteresis loops of the as-prepared α-Fe_2O_3 nanoparticles and exhibited a magnetic saturation (M_s) of 3.022 and 2.147 emu/g with coercivity (H_c) of 886 and 912 Oe, respectively [9,16,18,19]. The M_s value of α-Fe_2O_3 nanoparticles prepared from $Fe_2(SO_4)_3$ is more than the M_s value of α-Fe_2O_3 nanoparticles prepared from $Fe(NO_3)_3{\cdot}9H_2O$, since generally magnetic properties depend upon the synthesis technique, morphology, and size of particles [9,20,44].

The TEM images of the as-prepared α-Fe_2O_3 nanoparticles are illustrated in Fig. 4. It can be seen that their morphologies are found to be nearly spherical in shape with different sizes. However, the average size of α-Fe_2O_3 nanoparticles prepared from $Fe_2(SO_4)_3$ is smaller than the size of α-Fe_2O_3 nanoparticles prepared from $Fe(NO_3)_3{\cdot}9H_2O$. In addition, the particles prepared were highly agglomerated and a high crystallinity emerged [9].

Usually, the surface of transition metal oxides is exposed to hydroxyl groups that can act as a functional group for them [11]. Then, the charge surface of transition metal oxides depends on the pH solution. The point of zero charge (PZC) of the transition metal oxides usually does not depend on the crystalline shapes and sizes and for α-Fe_2O_3 nanoparticles calculated at about 8-9; however, it is very sensitive to any impurities in the surface of materials as well as temperature [11]. The surface of α-Fe_2O_3 nanoparticles has an overall positive charge due to the formation of $FeOH_2^+$ at a pH below PZC and is negative charge due to the formation of FeO^- at a pH higher than PZC [11]. The Zeta potential of the α-Fe_2O_3 nanoparticles measured in aqueous solution is shown in Fig. 5. The iso-electric point is 8.19 for α-Fe_2O_3 nanoparticles prepared from $Fe(NO_3)_3{\cdot}9H_2O$, and 8.434 for α-Fe_2O_3 nanoparticles prepared from $Fe_2(SO_4)_3$.

Specific surface area and pore diameter distribution of the as-prepared α-Fe_2O_3 nanoparticles were analyzed by N_2 adsorption-desorption isotherms and were given in Fig. 6. As shown in Fig. 6, the N_2 adsorption-desorption curves similar to type III and the hysteresis loops (H3) are at P/P_o = 0.27, indicating micropores structure for the samples. The surface area of α-Fe_2O_3 nanoparticles prepared from $Fe(NO_3)_3{\cdot}9H_2O$ and $Fe_2(SO_4)_3$ are 3.1278 and 7.4525 m^2/g, respectively, confirming the smaller size of α-Fe_2O_3 nanoparticles prepared from $Fe_2(SO_4)_3$ than $Fe(NO_3)_3{\cdot}9H_2O$. Table 1 presents the BET data for α-Fe_2O_3 nanoparticles.

Table 1. BET data for α-Fe_2O_3 nanoparticles

Sample prepared from	$Fe(NO_3)_3{\cdot}9H_2O$	$Fe_2(SO_4)_3$
V_m [cm^3(STP) g^{-1}]	0.7186	1.7122
$a_{s,BET}$ [m^2 g^{-1}]	3.1278	7.4525
Total pore volume(p/p_0=0.990) [cm^3 g^{-1}]	0.010372	0.0072754
Mean pore diameter [nm]	13.264	3.9049

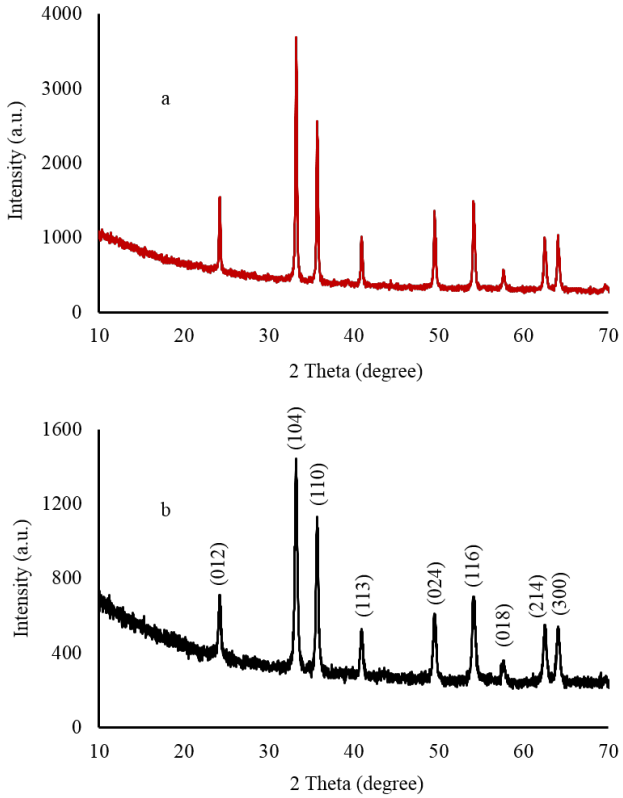

Fig. 2. XRD patterns of α-Fe_2O_3 prepared from a) $Fe(NO_3)_3{\cdot}9H_2O$, and b) $Fe_2(SO_4)_3$

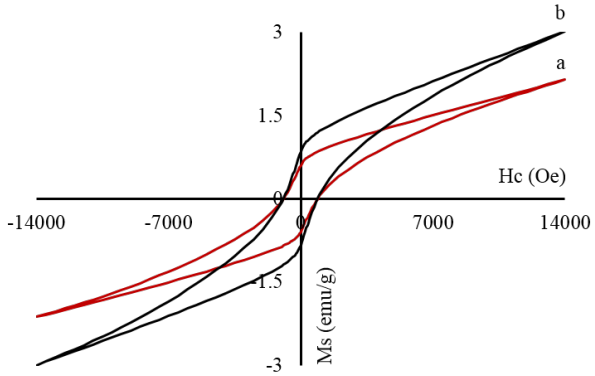

Fig. 3. Magnetic hysteresis loops of α-Fe_2O_3 prepared from a) $Fe(NO_3)_3{\cdot}9H_2O$, and b) $Fe_2(SO_4)_3$

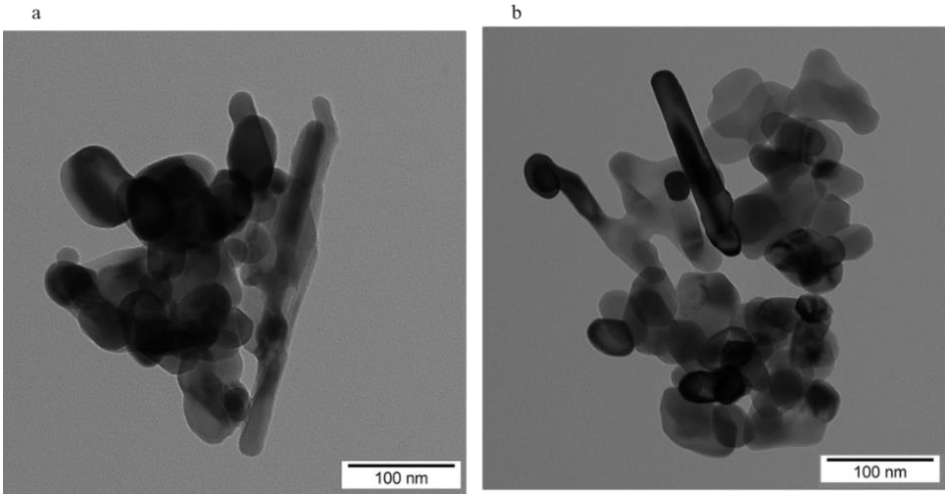

Fig. 4. TEM images of α-Fe_2O_3 prepared from a) $Fe(NO_3)_3{\cdot}9H_2O$, and b) $Fe_2(SO_4)_3$

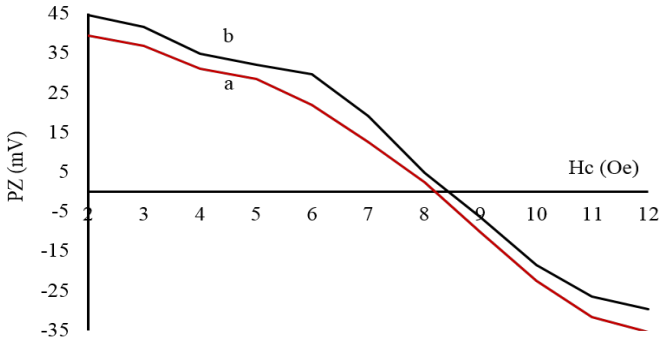

Fig. 5. Zeta potential of α-Fe_2O_3 prepared from a) $Fe(NO_3)_3{\cdot}9H_2O$, and b) $Fe_2(SO_4)_3$

Photocatalytic methyl orange (MO) degradation

Finally, the as-prepared α-Fe_2O_3 nanoparticles have been used for the photocatalytic degradation of methyl orange (MO) under the visible light irradiation. Initial pH solution is one of the best parameters for the photodegradation of MO using different photocatalyst [13,19,45]. According to the zeta potential results (Fig. 5), the surface partial charge of as-synthesized α-Fe_2O_3 nanoparticles is positive at pH solution below ≈8.3. Due to the greater adsorption capacity of MO molecules as anionic dye on the positively charged catalyst, resulting in a best contact between photogenerated radical species and surface of the catalyst and increasing the rate of photodegradation of MO at low pH (Fig. 7).

Fig. 8 illustrates the effect of irradiation time on the degradation percentage of MO in the presence of 0.005, 0.01 and 0.02 g of photocatalysts at a pH solution of 3. The degradation percentage of MO was measured using the following equation, where C_o and C_t are the initial and given time concentration of MO, respectively.

Degradation percentage (%) = $\{(C_o-C_t)/C_o\} \times 100$

Firstly, the results in Fig. 8 demonstrate that the as-synthesized α-Fe_2O_3 nanoparticles prepared from $Fe(NO_3)_3{\cdot}9H_2O$ and $Fe_2(SO_4)_3$ degraded about 84.3% and 96.8% of MO after 120 min of visible light irradiation, predicting the high efficiency of the samples, similar to previous reports [13,14,18-20,46]. The degradation speed of MO is very fast at a time range of 5-30 min and after that the degradation becomes slower due the decrease of MO concentration and also the obstruction of active site surface of the as-synthesized α-Fe_2O_3 nanoparticles. In addition, the degradation efficiency of MO increases by rising the photocatalyst dose from 0.005 to 0.02 g. We found that the final solution was colorless

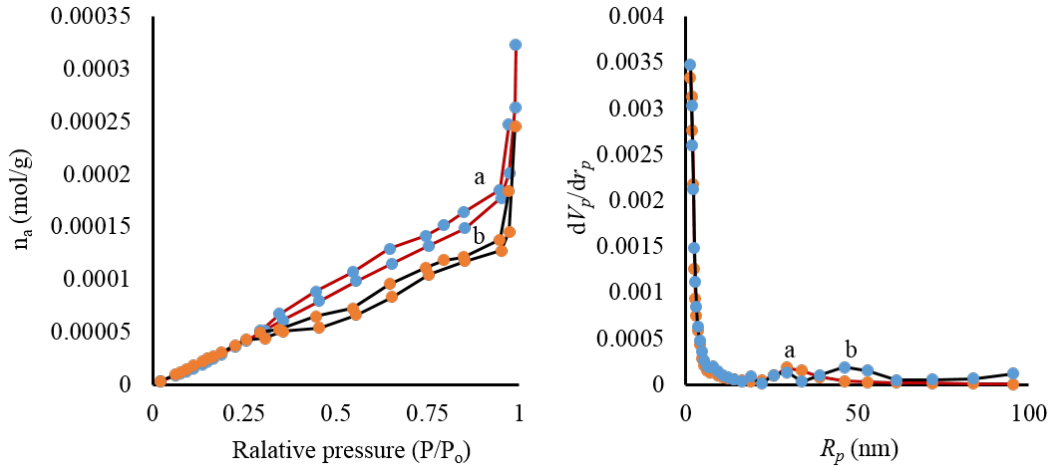

Fig. 6. N_2 adsorption-desorption isotherms and pore size distribution of α-Fe_2O_3 prepared from a) $Fe(NO_3)_3{\cdot}9H_2O$, and b) $Fe_2(SO_4)_3$

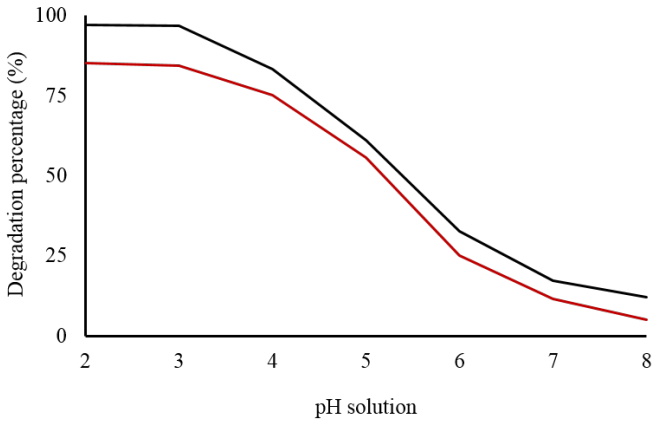

Fig. 7. Effect of pH solution on degradation percentage of MO in presence of 0.02 g of photocatalysts using α-Fe_2O_3 prepared from a) $Fe(NO_3)_3{\cdot}9H_2O$, and b) $Fe_2(SO_4)$

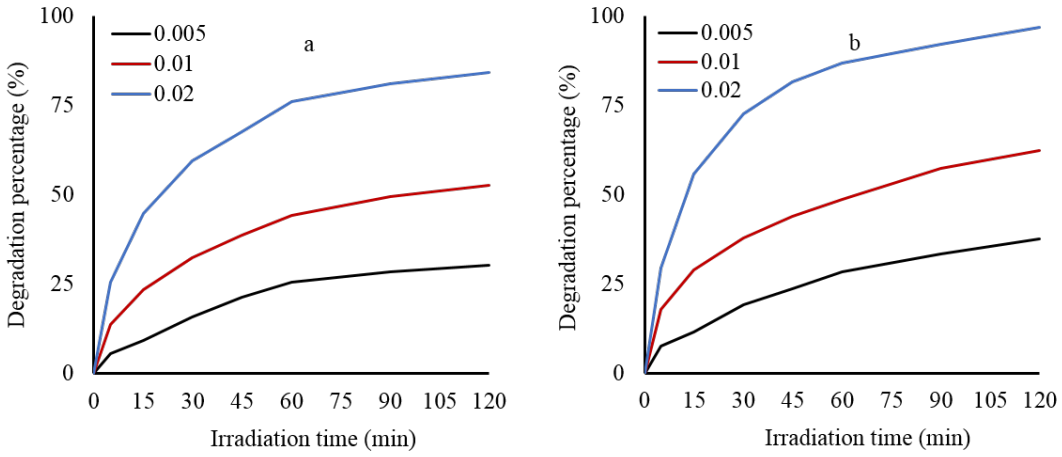

Fig. 8. Effect of irradiation time on degradation percentage of MO in presence of 0.005, 0.01 and 0.02 g of photocatalysts at a pH solution of 3 using α-Fe_2O_3 prepared from a) $Fe(NO_3)_3{\cdot}9H_2O$, and b) $Fe_2(SO_4)_3$

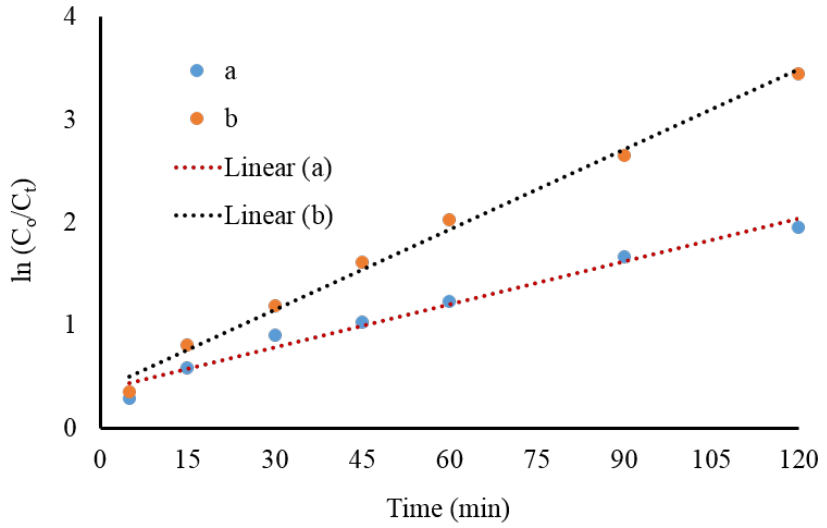

Fig. 9. Kinetic curves of photocatalytic degradation reaction of MO using α-Fe_2O_3 nanoparticles prepared from a) $Fe(NO_3)_3{\cdot}9H_2O$, and b) $Fe_2(SO_4)_3$

and the reddish brown solid produced from the degradation of MO was deposited on the surface of α-Fe_2O_3 nanoparticles as the photocatalyst of the bottom of Becker and was completely removed by the external magnetic field [46].

Finally, photocatalytic degradation reaction of MO using α-Fe_2O_3 nanoparticles prepared from $Fe(NO_3)_3{\cdot}9H_2O$ and $Fe_2(SO_4)_3$ follows Langmuir kinetic model (Fig. 9) using the following equation [46], where C_o represents the initial concentration and C_t denotes the concentration at time t, and *k* is the rate constant of the reaction.

$\ln (C_o/C_t) = kt$

The rate constant (k) of photocatalytic degradation reaction of MO can be calculated by the slope of fitting curves $\ln (C_o/C_t)$ versus time and are 0.01374 and 0.02689 min^{-1}, respectively, for α-Fe_2O_3 nanoparticles prepared from $Fe(NO_3)_3{\cdot}9H_2O$ and $Fe_2(SO_4)_3$. These results predicted that the photodegradation of the as-prepared α-Fe_2O_3 nanoparticles are higher than that of other forms of α-Fe_2O_3 nanoparticles [46] and is equal to that of other forms of α-Fe_2O_3 nanoparticles [18,19].

CONCLUSIONS

Summary, α-Fe_2O_3 nanoparticles were synthesized, characterized and used as a new catalyst for the photodegradation of methyl orange (MO) dye under visible light irradiation. The photodegradation results demonstrated the degradation efficiency of 84.3% and 96.8% for MO, after 120 min of visible light irradiation at an initial pH solution of 3. These results introduce the as-prepared α-Fe_2O_3 nanoparticles as a suitable and new candidate photocatalyst for the degradation of other organic dyes.

CONFLICT OF INTEREST

The authors declare no conflicts of interest.

REFERENCES

1. Moradnia F, Taghavi Fardood S, Ramazani A, Gupta VK. Green synthesis of recyclable MgFeCrO4 spinel nanoparticles for rapid photodegradation of direct black 122 dye. Journal of Photochemistry and Photobiology A: Chemistry. 2020;392:112433. https://doi.org/10.1016/j.jphotochem.2020.112433
2. Moradnia F, Taghavi Fardood S, Ramazani A, Osali S, Abdolmaleki I. Green sol-gel synthesis of CoMnCrO 4 spinel nanoparticles and their photocatalytic application. Micro & Nano Letters. 2020;15. https://doi.org/10.1049/mnl.2020.0189
3. Moradnia F, Taghavi Fardood S, Ramazani A, Min B-K, Joo S, Varma R. Magnetic Mg0.5Zn0.5FeMnO4 nanoparticles: Green sol-gel synthesis, characterization, and photocatalytic applications. Journal of Cleaner Production. 2020;288:125632. https://doi.org/10.1016/j.jclepro.2020.125632
4. Dara M, Hassanpour M, Alshamsi H, Baladi M, Salavati-Niasari M. Green sol-gel auto combustion synthesis and characterization of double perovskite Tb2ZnMnO6 nanoparticles and a brief study of photocatalytic activity. RSC Advances. 2021;11:8228-38. https://doi.org/10.1039/D0RA10400K
5. Ali A, Zafar H, Zia M, Haq I, Phull A, Sarfraz Ali J, et al. Synthesis, characterization, applications, and challenges of iron oxide nanoparticles. Nanotechnology, Science and Applications. 2016;Volume 9:49-67.

https://doi.org/10.2147/NSA.S99986
6. Wu W, He Q, Jiang C. Magnetic Iron Oxide Nanoparticles: Synthesis and Surface Functionalization Strategies. Nanoscale research letters. 2008;3:397-415. https://doi.org/10.1007/s11671-008-9174-9
7. Yarjanli Z, Ghaedi K, Esmaeili A, Rahgozar S, Zarrabi A. Iron oxide nanoparticles may damage to the neural tissue through iron accumulation, oxidative stress, and protein aggregation. BMC Neuroscience. 2017;18. https://doi.org/10.1186/s12868-017-0369-9
8. Mazrouaa A, Mohamed M, Fekry M. Physical and magnetic properties of iron oxide nanoparticles with different molar ratio of ferrous and ferric. Egyptian Journal of Petroleum. 2019;28. https://doi.org/10.1016/j.ejpe.2019.02.002
9. Lassoued A, Lassoued M, Dkhil B, Ammar S, Gadri A. Synthesis, photoluminescence and Magnetic properties of iron oxide (α-Fe2O3) nanoparticles through precipitation or hydrothermal methods. Physica E: Low-dimensional Systems and Nanostructures. 2018;101. https://doi.org/10.1016/j.physe.2018.04.009
10. Che Ku Hitam CK, Abdul Jalil A. A review on exploration of Fe2O3 photocatalyst towards degradation of dyes and organic contaminants. Journal of environmental management. 2020;258:110050. https://doi.org/10.1016/j.jenvman.2019.110050
11. Kusior A, Michalec K, Jelen P, Radecka M. Shaped Fe2O3 nanoparticles - Synthesis and enhanced photocatalytic degradation towards RhB. Applied Surface Science. 2019;476:342-52. https://doi.org/10.1016/j.apsusc.2018.12.113
12. Khurram R, Wang Z, Ehsan M. α-Fe2O3-based nanocomposites: synthesis, characterization, and photocatalytic response towards wastewater treatment. Environmental Science and Pollution Research. 2021;28:1-15. https://doi.org/10.1007/s11356-020-11778-w
13. Kassegn G, Sibhatu A. Photocatalytic activity of biosynthesized α-Fe2O3 nanoparticles for the degradation of methylene blue and methyl orange dyes. Optik. 2021;241:167226. https://doi.org/10.1016/j.ijleo.2021.167226
14. Gupta N, Ghaffari Y, Bae J, Kim K. Synthesis of coral-like α-Fe2O3 nanoparticles for dye degradation at neutral pH. Journal of Molecular Liquids. 2020;301:112473. https://doi.org/10.1016/j.molliq.2020.112473
15. Ye C, Hu K, Niu Z, Lu Y, Zhang L, Yan K. Controllable synthesis of rhombohedral α-Fe2O3 efficient for photocatalytic degradation of bisphenol A. Journal of Water Process Engineering. 2019;27:205-10. https://doi.org/10.1016/j.jwpe.2018.12.008
16. Araujo R, Pereira do Nascimento E, Firmino HCT, Macedo D, Neves G, Morales Torres M, et al. α-Fe2O3 fibers: An efficient photocatalyst for dye degradation under visible light. Journal of Alloys and Compounds. 2021;882:160683. https://doi.org/10.1016/j.jallcom.2021.160683
17. Subramanian K, Ravi G, Kumar P, Elshikh M, Alkhamis H, Alrefaei A, et al. A strategy to enhance the photocatalytic efficiency of α-Fe2O3. Chemosphere. 2021;270:129498. https://doi.org/10.1016/j.chemosphere.2020.129498
18. Khalaji AD, Machek P, Jarosova M. α-Fe2O3 nanoparticles: synthesis, characterization, magnetic properties and photocatalytic degradation of methyl orange. Advanced Journal of Chemistry-Section A. 2021;4(4):317-26.
19. Khalaji A. Spherical α-Fe2O3 Nanoparticles: Synthesis and Characterization and Its Photocatalytic Degradation of Methyl Orange and Methylene Blue. Physical Chemistry Research. 2022;10:473-83.
20. Gandha K, Mohapatra J, Hossain MK, Elkins K, Poudyal N, Rajeshwar K, et al. Mesoporous Iron Oxide Nanowires: Synthesis, Magnetic and Photocatalytic Properties. RSC Adv. 2016;6. https://doi.org/10.1039/C6RA18530D
21. Qiu M, Wang R, Qi X. Hollow polyhedral α-Fe2O3 prepared by self-assembly and its photocatalytic activities in degradation of RhB. Journal of the Taiwan Institute of Chemical Engineers. 2019;102. https://doi.org/10.1016/j.jtice.2019.05.024
22. Yuvaraja G, Chen D-Y, Pathak J, Long J, Venkata Subbaiah M, Wen J-C, et al. Preparation of novel aminated chitosan schiff's base derivative for the removal of methyl orange dye from aqueous environment and its biological applications. International Journal of Biological Macromolecules. 2019;146. https://doi.org/10.1016/j.ijbiomac.2019.09.236
23. Habiba U, Siddique T, Lee J, Tan CJ, Ang B, Afifi A. Adsorption study of Methyl orange by Chitosan/Polyvinyl Alcohol/Zeolite Electrospun Composite Nanofibrous Membrane. Carbohydrate Polymers. 2018;191. https://doi.org/10.1016/j.carbpol.2018.02.081
24. Thulasi singh A, P S, K S. Synthesis of nano-sized chitosan blended polyvinyl alcohol for the removal of Eosin Yellow dye from aqueous solution. Journal of Water Process Engineering. 2016;13:127-36. https://doi.org/10.1016/j.jwpe.2016.08.003
25. Sharma P, Saikia BK, Das M. Removal of methyl green dye molecule from aqueous system using reduced graphene oxide as an efficient adsorbent: Kinetics, isotherm and thermodynamic parameters. Colloids and Surfaces A: Physicochemical and Engineering Aspects. 2014;457:125-33. https://doi.org/10.1016/j.colsurfa.2014.05.054
26. Asmaa M, Ghelamallah M, Benghalem A. Sorptive Removal of Methyl Green from Aqueous Solutions using Acivated Bentonite2016.
27. Alardhi S, Albayati T, Alrubaye J. Adsorption of the methyl green dye pollutant from aqueous solution using mesoporous materials MCM-41 in a fixed-bed column. Heliyon. 2020;6:e03253. https://doi.org/10.1016/j.heliyon.2020.e03253
28. Cao Y, Alamri S, Rajhi A, Anqi A, Khalaji A. New chitosan Schiff base and its nanocomposite: Removal of methyl green from aqueous solution and its antibacterial activities. International Journal of Biological Macromolecules. 2021;192. https://doi.org/10.1016/j.ijbiomac.2021.09.192
29. Foroughnia A, Khalaji A, Kolvari E, Koukabi N. Synthesis of new chitosan Schiff base and its Fe2O3 nanocomposite: Evaluation of methyl orange removal and antibacterial activity. International Journal of Biological Macromolecules. 2021;177. https://doi.org/10.1016/j.ijbiomac.2021.02.068
30. Hsu N-F, Hsu K-T. A simple synthetic technique to produce ZnO/Fe2O3/Fe3O4 nanostructures and application as a photocatalyst. Iranian Journal of Catalysis. 2022;12:77-84.
31. Alikhani M, Saviz S, Sari A. Synthesis and Characterization ZnO-Fe2O3 Nanocomposite with Thermal Plasma Method. 2022.
32. Tran QTB, Pham DH, Ngo MNT, Pham TD, Doan TVH, Luong THV. Cuprous oxide nanocubes functionalized

with graphene quantum dots and its application for methylene blue degradation. Iranian Journal of Catalysis. 2022;12(1):85-95.
33. Sahu K, Singh J, Mohapatra S. Photocatalytic and catalytic removal of toxic pollutants from water using CuO nanosheets. Journal of Materials Science: Materials in Electronics. 2019;30(6):6088-99. https://doi.org/10.1007/s10854-019-00910-3
34. Jeon S, Ko J-W, Ko W. Synthesis of Gd2O3 Nanoparticles and Their Photocatalytic Activity for Degradation of Azo Dyes. Catalysts. 2021;11:742. https://doi.org/10.3390/catal11060742
35. Mohammadi K, Sadeghi M, Azimirad R. Facile synthesis of SrFe12O19 nanoparticles and its photocatalyst application. Journal of Materials Science: Materials in Electronics. 2017;28(14):10042-7. https://doi.org/10.1007/s10854-017-6763-3
36. Safat S, Buazar F, Albukhaty S, Matroodi S. Enhanced sunlight photocatalytic activity and biosafety of marine-driven synthesized cerium oxide nanoparticles. Scientific Reports. 2021;11(1):14734. https://doi.org/10.1038/s41598-021-94327-w
37. Sehar S, Naz I, Rehman A, Sun W, Alhewairini S, Zahid M, et al. Shape-controlled synthesis of cerium oxide nanoparticles for efficient dye photodegradation and antibacterial activities. Applied Organometallic Chemistry. 2020;35. https://doi.org/10.1002/aoc.6069
38. Saadoon SJ, Jarosova M, Machek P, Kadhim MM, Ali MH, Khalaji AD. Methylene blue photodegradation using as-synthesized CeO2 nanoparticles. Journal of the Chinese Chemical Society. 2022;69(2):280-8. https://doi.org/10.1002/jccs.202100476
39. Vatanparast M, Saedi L. Sonochemical-assisted synthesis and characterization of CeO2 nanoparticles and its photocatalytic properties. Journal of Materials Science: Materials in Electronics. 2018;29. https://doi.org/10.1007/s10854-018-8698-8
40. Lassoued A, Lassoued M, Dkhil B, Ammar S, Gadri A. Photocatalytic degradation of methyl orange dye by NiFe2O4 nanoparticles under visible irradiation: effect of varying the synthesis temperature. Journal of Materials Science: Materials in Electronics. 2018;29:1-11. https://doi.org/10.1007/s10854-018-8693-0
41. Yavari S, Mahmodi NM, Teymouri P, Shahmoradi B, Maleki A. Cobalt ferrite nanoparticles: Preparation, characterization and anionic dye removal capability. Journal of the Taiwan Institute of Chemical Engineers. 2016;59:320-9. https://doi.org/10.1016/j.jtice.2015.08.011
42. Taghavi Fardood S, Moradnia F, Moradi S, Forootan R, Yekke Zare F, Heidari M. Eco-friendly synthesis and characterization of α-Fe2O3 nanoparticles and study of their photocatalytic activity for degradation of Congo red dye. Nanochemistry Research. 2019;4(2):140-7.
43. Taghavi Fardood S, Moradnia F, Forootan R, Abbassi R, Jalalifar S, Ramazani A, et al. Facile green synthesis, characterization and visible light photocatalytic activity of MgFe2O4@CoCr2O4 magnetic nanocomposite. Journal of Photochemistry and Photobiology A: Chemistry. 2022;423:113621. https://doi.org/10.1016/j.jphotochem.2021.113621
44. Sharma S, Dhiman N, Kumar A, Singh M, Dhiman P. Effect of Synthesis Method on Optical and Magnetic Properties of Fe2O3 Nanoparticles. Integrated Ferroelectrics. 2020;204(1):38-46. https://doi.org/10.1080/10584587.2019.1674986
45. Hakimi M, Morvaridi M, Hosseini HA, Alimard P. Preparation, characterization, and photocatalytic activity of Bi2O3-Al2O3 nanocomposite. Polyhedron. 2019;170:523-9. https://doi.org/10.1016/j.poly.2019.06.029
46. Wang J, Shao X, Zhang Q, Tian G, Ji X, Bao W. Preparation of mesoporous magnetic Fe2O3 nanoparticle and its application for organic dyes removal. Journal of Molecular Liquids. 2017;248:13-8. https://doi.org/10.1016/j.molliq.2017.10.026